Parametric down-conversion with optimized spectral properties in nonlinear photonic crystals

María Corona and Alfred B. U'Ren
Centro de Investigación Científica y de Educación Superior de Ensenada (CICESE), Baja California 22860, Mexico
(Received 20 June 2007; published 18 October 2007)

We study the joint spectral properties of photon pairs generated by spontaneous parametric down-conversion in a one-dimensional nonlinear photonic crystal in a collinear, degenerate, type-II geometry. We show that the photonic crystal properties may be exploited to compensate for material dispersion and obtain photon pairs that are nearly factorable, in principle, for arbitrary materials and spectral regions, limited by the ability to fabricate the nonlinear crystal with the required periodic variation in the refractive indices for the ordinary and extraordinary waves.

DOI: 10.1103/PhysRevA.76.043829 PACS number(s): 42.50.Dv, 42.70.Qs

I. INTRODUCTION

Two-photon states with specific continuous-variable entanglement properties are required for a number of quantum-information-processing applications. In particular, pure-state single photons, crucial for applications relying on interference between independently prepared single photons, such as quantum computing with linear optics [1], entanglement swapping [2], and teleportation [3], can be heralded only from *factorable* photon pairs, where no correlations exist between the constituent single photons [4]. Let us note that factorability may be imposed by postselecting an appropriate subensemble of photon pairs through spectral and/or spatial filtering; this can be done only at the cost of a typically drastic reduction in count rate and source brightness. Scalable quantum-information processing requires the elimination of this type of postselection. It has furthermore been shown that, for quantum-information applications involving multiple-pair generation resulting from high-gain parametric down-conversion, spectral or spatial filtering is likewise ineffectual [5]. In addition, the coexistence of factorability and a large generated bandwidth is important for some applications, such as the generation of ultrashort Fourier-transform-limited heralded single photons [6]. The process of spontaneous parametric down-conversion represents a well-established method for the generation of photon pairs, leading to unparalleled flexibility in the resulting continuous-variable entanglement properties. Indeed, the nonlinear crystal dispersion characteristics in conjunction with temporal and spatial structure in the pump beam may be exploited to engineer the type and degree of correlations present in spectral and transverse wave-vector degrees of freedom *at the source*, thus eliminating the need for photon pair filtering.

The use of a broadband pump is essential in the context of the generation of photon pairs with spectrally engineered properties; indeed, a monochromatic pump can access only a one-dimensional subspace of signal-idler frequency space, which precludes certain states of interest. Previous work has established the central role that is played by group velocity mismatch terms between the three fields involved in parametric down-conversion (pump, signal, and idler) in the determination of the resulting photon pair properties. Thus, in Ref. [7], it was shown that if the pump pulse propagates at a higher group velocity than one of the generated photons but lower than the conjugate generated photon, then it becomes possible to emit factorable photon pairs. An important limitation of this technique is that the group velocity condition which must be satisfied occurs only for specific materials, at specific spectral ranges [8,9], typically in the infrared where single-photon detection is unfortunately not well developed. A number of techniques have been proposed and in some cases implemented which enable effective control over the photon pair entanglement properties in the spectral domain unconstrained by material dispersion. In one such technique, the effective group velocities experienced by the three fields involved are modified by the angular dispersion introduced by a pair of diffraction gratings placed before and after the nonlinear crystal so as to generate photon pairs with tunable spectral characteristics [10,11]. Alternatively, the spectral content of two photon states may be restricted to the modes supported by a nonlinear cavity which leads, for a short, high-finesse cavity, to factorable, narrowband photon pair generation [12]. Likewise, on the one hand a transversely pumped source where signal and idler photons are emitted in a counterpropagating waveguided geometry [13] and on the other hand noncollinear parametric down-conversion (PDC) where a specific relationship between transverse and longitudinal phase matching is attained [14] can both lead to states with spectrally engineered properties. Another route is the use of crystal superlattices, where the dispersion in short crystal segments is compensated by birefringent compensators, permitting two-photon states with a wide range of possible spectral entanglement characteristics [4,15].

Previous theoretical work has explored the use of nonlinear photonic crystals in the context of the process of spontaneous parametric down-conversion. In particular, Refs. [16,17] study the potential of semiconductor-based nonlinear one-dimensional photonic crystals to yield phase-matching properties appropriate for the generation of polarization-entangled photon pairs. Likewise, it has been shown that even a short one-dimensional photonic crystal is capable of generating a considerable photon pair flux due to field localization in such structures [18–20]. In this paper we study the potential of exploiting the properties of one-dimensional nonlinear photonic crystals in order to generate photon pairs with engineered spectral entanglement properties. We concentrate on type-II, frequency degenerate, collinear PDC. Collinear operation is important because it permits PDC in a waveguided geometry, which leads to larger generation rates

as well as to effective control over the transverse spatial structure of the emitted light, crucial for efficient single-mode fiber coupling and for spatial mode matching in interference experiments [21]. Type-II operation for which the signal and idler photons are orthogonally polarized is important because it enables efficient photon pair splitting. We show that a weak index of refraction modulation present in an otherwise standard birefringent nonlinear crystal can be exploited to attain the group velocity conditions, in addition to basic phase matching, required for factorable photon pair generation.

II. ONE-DIMENSIONAL NONLINEAR PHOTONIC CRYSTALS

In this paper we analyze the generation of photon pairs by the process of parametric down-conversion in a $\chi(2)$ material characterized by a spatial periodicity in its linear optical properties. In particular, we study PDC produced by a nonlinear photonic crystal (NLPC) based on a standard bulk nonlinear crystal with uniaxial birefringence which has been modified from its natural state by an appropriate physical mechanism so as to yield a periodic variation of the index of refraction for both polarizations, while maintaining the nonlinearity constant throughout the crystal thickness. Concretely, within one period of the resulting Bragg grating, we assume that the index of refraction for the ordinary ($\mu=o$) and the extraordinary ($\mu=e$) rays are given by

$$n_\mu(\omega,z) = \begin{cases} n_{\mu 1}(\omega), & 0 < z < a, \\ n_{\mu 2}(\omega), & a < z < \Lambda. \end{cases} \tag{1}$$

This unit cell is assumed to be replicated throughout the crystal length. Here, Λ represents the Bragg period and a/Λ is the duty cycle. We refer to such a material as a one-dimensional nonlinear photonic crystal. Figure 1 shows a crystal schematic where A indicates zones characterized by indices of refraction n_{o1} and n_{e1} and B indicates zones characterized by indices of refraction n_{o2} and n_{e2}. We assume that in zones A the crystal has been left in its natural state, while in zones B it has undergone index change. For simplicity, we assume that zones A and B are of equal length (leading to an $a/\Lambda=0.5$ duty cycle) and we likewise assume that the permittivity contrast α, equivalent to the index square contrast, is frequency independent,

$$\alpha = \frac{2[\epsilon_{\mu 1}(\omega) - \epsilon_{\mu 2}(\omega)]}{\epsilon_{\mu 1}(\omega) + \epsilon_{\mu 2}(\omega)} = \frac{n_{\mu 1}(\omega)^2 - n_{\mu 2}(\omega)^2}{\bar{n}_\mu(\omega)^2}, \tag{2}$$

where

$$\bar{n}_\mu(\omega)^2 = [n_{\mu 1}(\omega)^2 + n_{\mu 2}(\omega)^2]/2 \tag{3}$$

with $\mu=e,o$. Throughout this paper we will assume that propagation of the three fields involved is normal to each of the interfaces between zones A and B. Under these conditions, such a material can exhibit, for each of the polarizations, a so-called photonic band gap centered at each of the Bragg wavelengths,

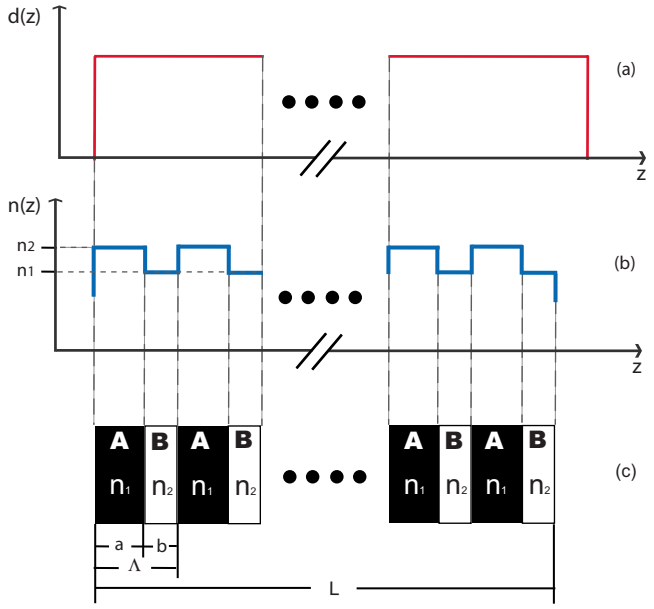

FIG. 1. (Color online) Schematic of a one-dimensional, nonlinear photonic crystal. (a) Second-order nonlinearity. (b) Refractive index, shown for one of the polarizations. (c) Representation of the periodic material, with $b=\Lambda-a$.

$$\lambda_\mu^{Bragg,m} = 2\bar{n}_\mu\Lambda/m, \tag{4}$$

where $m=1,2,3,\ldots$, and where $\mu=e,o$. Within each band gap, for a sufficient crystal thickness, light is efficiently reflected, while for frequencies outside the band gap, light propagates in the form of so-called Bloch waves, which can be written as

$$E(z,t) = E_K(z)\exp\{i[K(\omega)z - \omega t]\}. \tag{5}$$

Here, $E_K(z)$ is the Bloch envelope, which exhibits a spatial periodicity matching that of the material, i.e., $E_K(z+\Lambda)=E_K(z)$, while $K(\omega)$ represents the Bloch wave number. Note that, for a continuous material without Bragg grating, the Bloch envelope reduces to a constant, and therefore the Bloch wave reduces to a plane wave. Following a coupled-mode analysis where the spatial periodicity in the permittivity is assumed to be well represented by a weak perturbation to the material permittivity, it can be shown that the Bloch wave number in the vicinity of $K=m\pi/\Lambda$ can be expressed as [22]

$$K_\mu^{(m)}(\omega) = \pi m/\Lambda \pm \sqrt{(\Delta\beta_\mu^{(m)}/2)^2 - |\kappa_\mu^{(m)}|^2}. \tag{6}$$

Here, $\kappa_\mu^{(m)}$ represents the coupling coefficient between the forward and backward waves,

$$\kappa_\mu^{(m)} = i[1-\cos(m\pi)]\alpha\bar{k}_\mu(\omega)/(4\pi m), \tag{7}$$

and $\Delta\beta_\mu^{(m)}$ represents the Bragg phase mismatch between these two waves,

$$\Delta\beta_\mu^{(m)} = 2\bar{k}_\mu(\omega) - 2\pi m/\Lambda, \tag{8}$$

where $\bar{k}_\mu=\bar{n}_\mu\omega/c$ characterizes the underlying material dispersion; note that Eq. (4) follows from the condition $\Delta\beta^{(m)}$

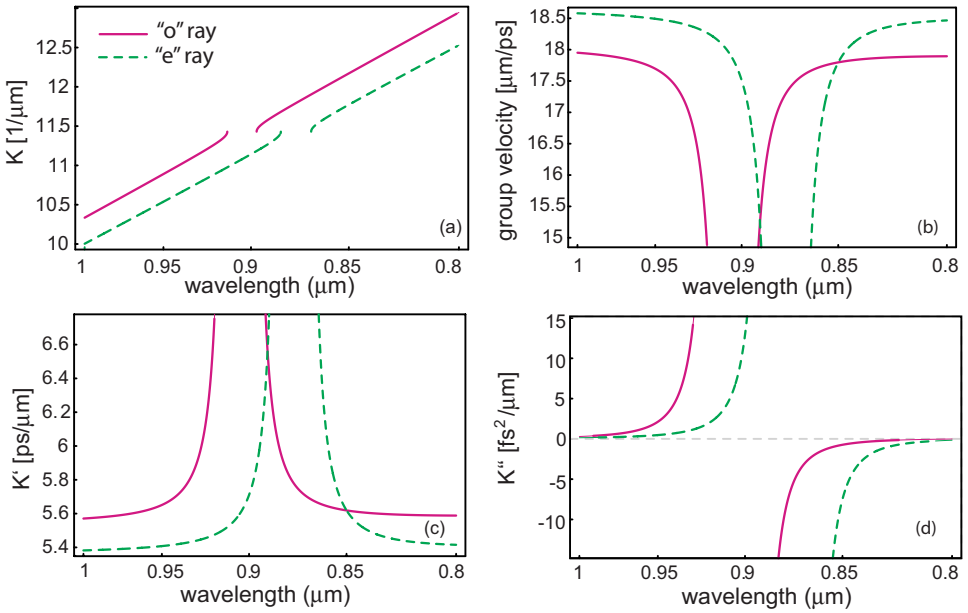

FIG. 2. (Color online) Plots as a function of frequency of (a) the Bragg wave number $K(\omega)$, (b) the group velocity $1/K'(\omega)$, (c) $K'(\omega)$, and (d) group velocity dispersion coefficient $K''(\omega)$; for comparison, the dotted horizontal line indicates the magnitude of the GVD coefficient for SF-10, a particularly dispersive glass.

$=0$. A photonic band gap appears when $\kappa_\mu^{(m)} \neq 0$ and its effects become appreciable for $\Delta\beta_\mu^{(m)} \approx 0$. The band-gap boundaries ω_{min} and ω_{max} are obtained by solving for the frequencies such that the argument of the square root in Eq. (6) vanishes. For a forward-propagating wave, the minus sign in front of the square root in Eq. (6) should be used for $\omega < \omega_{min}$ while the plus sign should be used for $\omega > \omega_{max}$. Let us note that, for a 0.5 duty cycle, Eq. (7) tells us that even-order band gaps $(m=2,4,6,\ldots)$ are suppressed.

In what follows, we will concentrate on first-order $(m=1)$ band gaps, though the analysis below could be employed for any order. Note that for practical implementations it may be challenging to fabricate the required Bragg gratings with periods in the region of hundreds of nanometers compatible with modified dispersive characteristics in the visible; alternatively, it is possible to use longer periods, together with higher-order band gaps. The dispersive properties of NPLCs are characterized by the function $K(\omega)$, where from this point we omit the order superscript. For propagating waves at frequencies in the vicinity of the band-gap boundaries, $K(\omega)$ can differ substantially from the underlying material dispersion relation $\bar{k}(\omega)$. In particular, group velocities can be strongly reduced, while group velocity dispersion terms (as well as higher-order frequency derivatives of the wave number) can increase markedly from their values associated with material-only dispersion.

In order to illustrate these effects, let us consider a specific example of a one-dimensional NLPC, based on a β-barium-borate (BBO) crystal. We assume that the Bragg period is given by $\Lambda=279.1$ nm with an $a/\Lambda=0.5$ duty cycle, the angle subtended by the pump and the optic axis (to be referred to as the propagation angle) is 41.8°, and the permittivity contrast is $\alpha=0.027$. Figure 2 shows the resulting dispersive properties. Figure 2(a) shows, for each of the two polarizations, the Bloch wave number $K(\omega)$ as a function of frequency, showing clearly a band gap for each of the polarizations, within which $K(\omega)$ becomes complex valued. Figure 2(b) shows the group velocities for each of the two polarizations, exhibiting a marked reduction near the band-gap boundaries. Figure 2(c) shows the first frequency derivative of $K(\omega)$, or the reciprocal group velocity. Finally, Fig. 2(d) shows the group velocity dispersion (GVD) term for each of the polarizations. It is apparent from the plot that GVD can be greatly enhanced near the band-gap boundaries, and likewise that it is possible to obtain both positive and negative GVD.

III. PDC IN ONE-DIMENSIONAL PHOTONIC NONLINEAR CRYSTALS

Following a standard perturbative approach, the quantum state describing photon pairs produced by parametric down-conversion in the spontaneous limit may be expressed as

$$|\psi(t)\rangle \approx \left(1 + \frac{1}{i\hbar}\int_0^t dt' \hat{H}(t')\right)|\text{vac}\rangle, \tag{9}$$

where $|\text{vac}\rangle$ denotes the vacuum and $\hat{H}$ is the interaction Hamiltonian

$$\hat{H}(t) = \varepsilon_0 \int_V dV\, d(\vec{r}) \hat{E}_p^{(+)}(\vec{r},t) \hat{E}_s^{(-)}(\vec{r},t) \hat{E}_i^{(-)}(\vec{r},t) + \text{H.c.} \tag{10}$$

Here, V is the illuminated volume in the nonlinear medium, $d(\vec{r})$ is the second-order nonlinearity, and $\hat{E}_\mu(\vec{r},t)$ $(\mu = p,s,i)$ represents the electric field operators associated with each of the interacting fields. In a nonlinear photonic crystal, each of these fields is described by a Bloch wave. Thus, if we assume that the pump field is classical, it can be expressed as

$$\hat{E}_p^{(+)}(\vec{r},t) \to \int d\omega\, \alpha_p(\omega) E_{K_p}(z,\omega) \exp\{i[K_p(\omega)z - \omega t]\}, \tag{11}$$

in terms of the Bloch wave number $K_p(\omega)$, Bloch envelope $E_{K_p}(z,\omega)$, and spectral amplitude $\alpha_p(\omega)$. It is convenient to

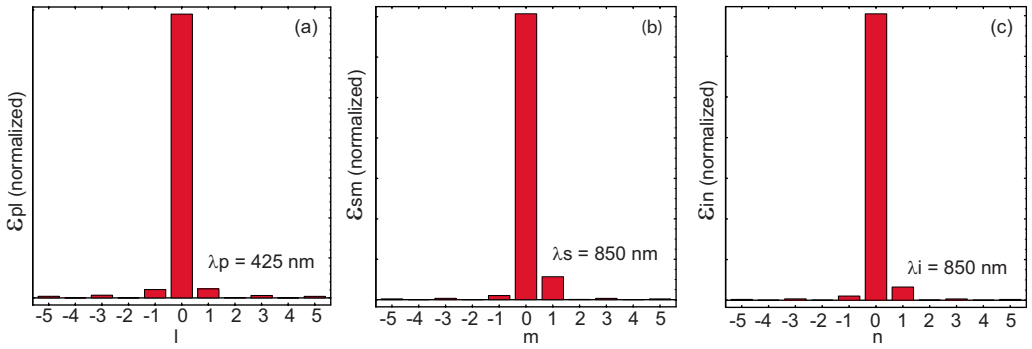

FIG. 3. (Color online) Normalized modulus of Fourier coefficients for (a) an extraordinary wave at 425 nm, (b) an extraordinary wave at 850 nm, and (c) an ordinary wave at 850 nm.

express the Bloch envelope as a Fourier series,

$$E_{K_p}(z,\omega) = \sum_l \varepsilon_{pl}(\omega) e^{iG_l z}, \tag{12}$$

in terms of the spatial harmonics $G_l = 2\pi l/\Lambda$. The signal and idler fields are quantized; their positive-frequency part can be expressed as

$$\hat{E}_\mu^{(+)}(\vec{r},t) = i \int d\omega \sum_l \varepsilon_{\mu l}(\omega) \ell_\mu(\omega) \hat{a}_\mu(K_\mu(\omega) + G_l) \times \exp(i\{[K_\mu(\omega) + G_l]z - \omega t\}) \tag{13}$$

in terms of the Bloch wave number $K_\mu(\omega)$ and the Bloch envelope Fourier series coefficients $\varepsilon_{\mu l}$. Here, $\ell_\mu(\omega) = \sqrt{\hbar\omega K'_\mu(\omega)/[2\epsilon_\mu(\omega)S]}$, where $K'_\mu(\omega)$ is the first frequency derivative of K_μ, $\hat{a}_\mu(K(\omega))$ is the annihilation operator for the signal (s) or idler (i) modes, $\varepsilon_\mu(\omega)$ is the permittivity in the nonlinear medium, and S is the transverse beam area.

It can be shown that the resulting two-photon component of the state may be written for specific directions of propagation (throughout this paper assumed to be collinear with the pump beam) as

$$|\Psi\rangle = \sum_{lmn} \int\int d\omega_s d\omega_i f_{lmn}(\omega_s,\omega_i) \times a_s^\dagger(K(\omega_s) + G_m) a_i^\dagger(K(\omega_i) + G_n)|\text{vac}\rangle, \tag{14}$$

where the joint spectral amplitude $f_{lmn}(\omega_s,\omega_i)$ may be factored as $f_{lmn}(\omega_s,\omega_i) = \alpha_p(\omega_s+\omega_i)\phi_{lmn}(\omega_s,\omega_i)$. Here, $\alpha_p(\omega_s+\omega_i)$ represents the pump spectral envelope function, while $\phi_{lmn}(\omega_s,\omega_i)$ is a function which describes the phase-matching properties of the nonlinear photonic crystal and can be expressed as

$$\phi_{lmn}(\omega_s,\omega_i) = \varepsilon_{pl}(\omega_s+\omega_i)\varepsilon^*_{sm}(\omega_s)\varepsilon^*_{in}(\omega_i) \times \ell_s(\omega_s)\ell_i(\omega_i)\text{sinc}(L\Delta K_{lmn}/2) \times \exp(iL\Delta K_{lmn}/2), \tag{15}$$

in terms of the frequency-dependent phase mismatch ΔK_{lmn} adjusted by the momentum contribution due to the photonic crystal structure,

$$\Delta K_{lmn} = \Delta K + 2\pi(l-m-n)/\Lambda \tag{16}$$

where $\Delta K = K_p - K_s - K_i$. The term proportional to $2\pi/\Lambda$ is similar to that which appears for quasi-phase-matched interactions and has the effect of shifting the spectral range where phase matching is attained. Thus, the phase-matching contributions for different values of $l-m-n$, if they exist (i.e., if $\Delta K_{lmn}=0$), will tend to be spectrally distinct from each other. Note, however, that in general terms, for photonic crystal periods in the hundreds of nanometers, contributions with $l-m-n \neq 0$ result in a term proportional to $2\pi/\Lambda$ which will tend to be larger than the wave numbers for each of the three interacting fields, and will therefore also be larger in absolute value than ΔK; this makes it difficult to achieve $\Delta K_{lmn}=0$ for $l-m-n \neq 0$.

Let us now consider the Bloch wave characteristics at 425 and 850 nm (which could represent pump and PDC wavelengths) in a material with the parameters specified at the end of the previous section. Figure 3 shows the modulus of the leading Fourier series coefficients [see Eqs. (12) and (13)], calculated from the Bloch envelope, in turn determined by the eigenvectors of the translation matrix which characterizes the periodic material [22]. Figure 3(a) shows the Fourier coefficients for an extraordinary wave at 425 nm, Fig. 3(b) shows the Fourier coefficients for an extraordinary wave at 850 mm, and Fig. 3(c) shows the Fourier coefficients for an ordinary wave at 850 mm. Let us note that a wave at 425 nm behaves essentially like a plane wave with negligible $l \neq 0$ terms. This is due to the fact that for this specific material there is no band gap in the vicinity of 425 nm; in particular, the second-order band gap is suppressed by employing an $a/\Lambda = 0.5$ duty cycle. This specific material exhibits a band gap centered at 904.9 nm for the ordinary wave and at 876.3 nm for the extraordinary wave. A wave of either polarization at 850 nm is sufficiently near to the corresponding band gap that the resulting dispersion relation is significantly modified (see Fig. 2), yet as observed in Figs. 3(b) and 3(c) they behave essentially as plane waves with small $m=1$ and $n=1$ (i.e., reflected wave) contributions and where other contributions are negligible.

In what follows, we will study the generation of PDC where the emission frequency is in sufficient proximity to the band-gap boundaries so that dispersion is strongly modified, though sufficiently removed so that the fraction of light ap-

pearing in modes other than the fundamental mode (determined by the values of m,n) is small; see Figs. 2 and 3. In this regime the signal and idler photons propagate essentially as plane waves, yet with a modified dispersion relation with respect to an equivalent source without a photonic crystal structure. From Eq. (7) there is no second-order band gap for a 0.5 duty cycle, which implies that the effect of the photonic crystal tends to be insignificant for the pump field, making contributions with $l \neq 0$ negligible. Thus, in this paper, we will concentrate on the contribution $l=m=n=0$, which corresponds to the fundamental, forward-propagating mode for the three interacting fields.

IV. CONDITIONS FOR FACTORIZABILITY

In order to carry out an analysis of the relationship between the various experimental parameters and the resulting spectral entanglement properties, it is convenient to express the phase mismatch as a power series in the frequency detunings $\nu_{s,i}=\omega_{s,i}-\omega_o$, where ω_o is the degenerate frequency and L is the crystal length,

$$L\Delta K \approx L\Delta K^{(0)} + \sum_{j=1}^{4} (\tau_s^{(j)}\nu_s^j + \tau_i^{(j)}\nu_i^j) + [2\tau_p^{(2)} + 3\tau_p^{(3)}(\nu_s+\nu_i) + 2\tau_p^{(4)}(2\nu_i^2 + 3\nu_s\nu_i + 2\nu_s^2)]\nu_s\nu_i + \vartheta(5). \quad (17)$$

Here, $\vartheta(5)$ represents fifth- and higher-order terms in the detunings while $\Delta K^{(0)}$ represents the frequency-independent term, which vanishes when perfect phase matching occurs at ω_o,

$$\Delta K^{(0)} = K_s(\omega_o) + K_i(\omega_o) - K_p(2\omega_o). \quad (18)$$

Equation (17) is written in terms of the mismatch in the jth frequency derivative of the wave number between the pump and the signal and idler wave packets $\tau_{s,i}^{(j)}$, and a term proportional to the jth frequency derivative of the pump wave number $\tau_p^{(j)}$,

$$\tau_\mu^{(j)} = L(K_p^{(j)} - K_\mu^{(j)}),$$

$$\tau_p^{(j)} = LK_p^{(j)}, \quad (19)$$

in terms of

$$K_\mu^{(j)} = (1/j!)\,(d^j K_\mu/d\omega^j)\big|_{\omega=\omega_o},$$

$$K_p^{(j)} = (1/j!)\,(d^j K_p/d\omega^j)\big|_{\omega=2\omega_o}. \quad (20)$$

Let us note that for type-II PDC in standard nonlinear crystals it is typically sufficient to consider a power series expansion of the phase mismatch up to the group velocity terms. However, for NLPCs with the signal and idler frequencies in proximity to one of the band-gap boundaries, GVD and higher-order dispersion terms are strongly enhanced with respect to an equivalent source without a photonic crystal structure. Thus, it becomes necessary to consider higher-order terms; here we have considered up to quartic order in the frequency detunings.

In order to facilitate an analysis of the conditions under which it is possible to generate two-photon states that are close to factorable, we write down the joint spectral amplitude in terms of Gaussian functions. This can be achieved by modeling the pump envelope function as a Gaussian function,

$$\alpha_p(\omega_s+\omega_i) = \exp[-(\omega_s+\omega_i-2\omega_o)^2/\sigma^2], \quad (21)$$

and by approximating the sinc function in the phase-matching function as a Gaussian function, i.e., $\mathrm{sinc}(x) \approx \exp(-\gamma x^2)$ with $\gamma \approx 0.193$. Under these approximations, the joint spectral amplitude can be expressed as

$$f(\nu_s,\nu_i) \approx \exp\{-(\gamma/4)[L^2\Delta K^2 + 4(\nu_s+\nu_i)^2/(\gamma\sigma^2)] + iL\Delta K/2\}. \quad (22)$$

By writing $L\Delta K$ in Eq. (22) as its power series expansion [Eq. (17)], and keeping terms up to fourth order while assuming that $\Delta K^{(0)}=0$, the joint spectral amplitude becomes

$$f(\nu_s,\nu_i) \approx \exp\{-(\gamma/4)[\Phi_s(\nu_s) + \Phi_i(\nu_i) + \Phi_{si}(\nu_s,\nu_i)]\} \quad (23)$$

where

$$\Phi_\mu(\nu) = [(\tau_\mu^{(1)})^2 + 4/(\gamma\sigma^2)]\nu^2 + 2\tau_\mu^{(1)}\tau_\mu^{(2)}\nu^3 + [(\tau_\mu^{(2)})^2 + 2\tau_\mu^{(1)}\tau_\mu^{(3)}]\nu^4 - i(2/\gamma)\sum_{j=1}^{4}\tau_\mu^{(j)}\nu^j \quad (24)$$

and

$$\Phi_{si}(\nu_s,\nu_i)/(2\nu_s\nu_i) = \tau_s^{(1)}\tau_i^{(1)} + 4/(\gamma\sigma^2) + (2\tau_p^{(2)}\tau_s^{(1)} + \tau_s^{(2)}\tau_i^{(1)})\nu_s + (2\tau_p^{(2)}\tau_i^{(1)} + \tau_i^{(2)}\tau_s^{(1)})\nu_i + (2\tau_p^{(2)}\tau_s^{(2)} + 3\tau_p^{(3)}\tau_s^{(1)} + \tau_s^{(3)}\tau_i^{(1)})\nu_s^2 + (2\tau_p^{(2)}\tau_i^{(2)} + 3\tau_p^{(3)}\tau_i^{(1)} + \tau_i^{(3)}\tau_s^{(1)})\nu_i^2 + [2(\tau_p^{(2)})^2 + \tau_s^{(2)}\tau_i^{(2)} + 3\tau_p^{(3)}(\tau_s^{(1)} + \tau_i^{(1)})]\nu_s\nu_i - i(2/\gamma)[\tau_p^{(2)} + (3/2)\tau_p^{(3)}(\nu_s+\nu_i) + \tau_p^{(4)}(2\nu_s^2 + 3\nu_s\nu_i + 2\nu_i^2)]. \quad (25)$$

While $\Phi_\mu(\nu)$ (with $\mu=s,i$) represents the contributions that depend only on one of the two frequencies, $\Phi_{si}(\nu_s,\nu_i)$ depends on both frequencies, and gives rise to correlations in the two-photon state; factorability is attained if $\Phi_{si}(\nu_s,\nu_i)=0$. It is apparent from Eqs. (24) and (25) that the dominant terms which govern the phase-matching behavior are the

group velocity mismatch terms, proportional to $\tau_{s,i}^{(1)}$. Let us consider the effect of making both of these group velocity mismatch terms vanish, i.e.,

$$\tau_s^{(1)} = \tau_i^{(1)} = 0. \tag{26}$$

In this case, for which the pump, signal, and idler propagate at the same group velocity, the expression for the joint spectral amplitude greatly simplifies, and in particular many of the mixed terms giving rise to correlations are suppressed. The modulus of the joint spectral amplitude becomes

$$\begin{aligned} |f(\nu_s,\nu_i)| \approx & \exp[-\nu_s^2/\sigma^2 - \gamma(\tau_s^{(2)})^2\nu_s^4/4] \\ & \times \exp[-\nu_i^2/\sigma^2 - \gamma(\tau_i^{(2)})^2\nu_i^4/4] \\ & \times \exp\{-2\nu_s\nu_i/\sigma^2 + \gamma\tau_p^{(2)}(\tau_s^{(2)}\nu_s^3\nu_i + \tau_i^{(2)}\nu_s\nu_i^3) \\ & + \gamma[(\tau_p^{(2)})^2 + \tau_s^{(2)}\tau_i^{(2)}/2]\nu_s^2\nu_i^2\}, \end{aligned} \tag{27}$$

while the argument becomes

$$\begin{aligned} \arg[f(\nu_s,\nu_i)] \approx & (1/2)\sum_{j=2}^{4}(\tau_s^{(j)}\nu_s^j + \tau_i^{(j)}\nu_i^j) + \nu_s\nu_i[\tau_p^{(2)} + 3\tau_p^{(3)}(\nu_s \\ & + \nu_i) + 2\tau_p^{(4)}(2\nu_s^2 + 3\nu_s\nu_i + 2\nu_i^2)]. \end{aligned} \tag{28}$$

Equation (27) is written as a product of three exponentials, where the first two represent the factorable components and the third term describes spectral (modulus) correlations between the signal and idler photons. Likewise, in Eq. (28) it is the second term, with a $\nu_s\nu_i$ overall multiplicative factor, which describes spectral phase correlations between the signal and idler photons.

Let us now in addition suppose that the signal and idler photons experience much stronger dispersion than the pump. In particular, let us assume that jth-order pump dispersion coefficients $\tau_p^{(j)}$ may be neglected with respect to the signal and idler jth-order dispersion coefficients $\tau_{s,i}^{(j)}$, i.e.,

$$|\tau_p^{(j)}| \ll |\tau_s^{(j)}|, |\tau_i^{(j)}|. \tag{29}$$

It may be shown that, if the condition in Eq. (29) with $j=2$ is satisfied, the fourth-order mixed terms in Eq. (27) proportional to $\tau_p^{(2)}$ may be neglected. Similarly, if the condition in Eq. (29) with $j=2,3,4$ is satisfied, the mixed terms in the argument of the joint amplitude [Eq. (28)] may be neglected. Imposing this weak pump dispersion condition, the expression for the joint spectral amplitude is thus further simplified. The modulus may now be written as

$$|f(\nu_s,\nu_i)| \approx \exp[-(\nu_s+\nu_i)^2/\sigma^2 - (\gamma/4)(\tau_s^{(2)}\nu_s^2 + \tau_i^{(2)}\nu_i^2)^2] \tag{30}$$

while the argument may be written as

$$\arg[f(\nu_s,\nu_i)] \approx (1/2)\sum_{j=2}^{4}(\tau_s^{(j)}\nu_s^j + \tau_i^{(j)}\nu_i^j). \tag{31}$$

Let us note that, while the modulus contains mixed terms proportional to $\nu_s\nu_i$ and to $\nu_s^2\nu_i^2$, the argument does not contain mixed terms. Let us now assume, in addition to group velocity matching [see Eq. (26)] and weak pump dispersion [see Eq. (29)], that the pump is broadband. It may be shown from Eq. (30) that the joint spectral amplitude exhibits no dependence on the pump bandwidth if

$$\sigma \gg 2(4/\gamma)^{1/4}(\tau_s^{(2)} + \tau_i^{(2)})^{-1/2}. \tag{32}$$

Thus, for a sufficiently broadband pump [so that Eq. (32) is satisfied], the modulus of the joint spectral amplitude reduces to

$$|f(\nu_s,\nu_i)| \approx \exp[-(\gamma/4)(\tau_s^{(2)}\nu_s^2 + \tau_i^{(2)}\nu_i^2)^2]. \tag{33}$$

We have seen that when the following three conditions are satisfied: (1) complete group velocity matching [see Eq. (26)], (2) weak pump dispersion [see Eq. (29)], and (3) sufficiently broadband pump [see Eq. (32)], the joint spectral amplitude attains a particularly simple form in which there is a single mixed term, proportional to $\nu_s^2\nu_i^2$ (up to fourth order in Δk^2). For the specific cases we analyzed (see the next section), while conditions 1 and 3 must be satisfied in order to attain nearly factorable two-photon states, the effect of the mixed terms controlled by condition 2 is comparatively small. As will be illustrated with a specific example in the following section, a joint spectral amplitude which approaches the functional form of Eq. (33) can describe a nearly factorable two-photon state. In this case, the ratio $\tau_s^{(2)}/\tau_i^{(2)}$ controls the degree of elongation and orientation (horizontal or vertical) of the joint spectral intensity in $\{\omega_s,\omega_i\}$ space. Thus, with favorable dispersive properties, it becomes possible to generate states ranging from those with equal bandwidths for signal and idler to highly elongated ones.

In the next section, we will show that the properties of one-dimensional nonlinear photonic crystals may be exploited for the fulfillment of conditions 1 and 3, and partial fulfillment of condition 2.

V. FULFILLMENT OF CONDITIONS WITH NONLINEAR PHOTONIC CRYSTALS

Our strategy for controlling the spectral properties of PDC photon pairs generated by one-dimensional NLPCs is based on the observation that the group velocity is sharply reduced for frequencies in the vicinity of the band-gap boundaries, as illustrated in Fig. 2(b). It is possible to exploit the properties of photonic crystals to compensate for material dispersion and to impose specific conditions on the group velocities of the three interacting fields. Indeed, while for a standard optical material the pump will tend to propagate at a lower group velocity than the generated light, it is possible to design a NLPC so that the group velocities of the signal and idler photons in proximity to one of the band-gap boundaries are reduced sufficiently to make them equal to the pump group velocity. The former can be achieved while maintaining essentially a plane-wave character for the corresponding signal and idler Bloch waves. Likewise, the NLPC can be designed so that the pump frequency is far from band gaps, so that the pump field is essentially unaffected by the photonic crystal structure. Indeed, NLPCs make it possible to attain, even in a type-II geometry where each of the three fields experiences different dispersion characteristics, complete

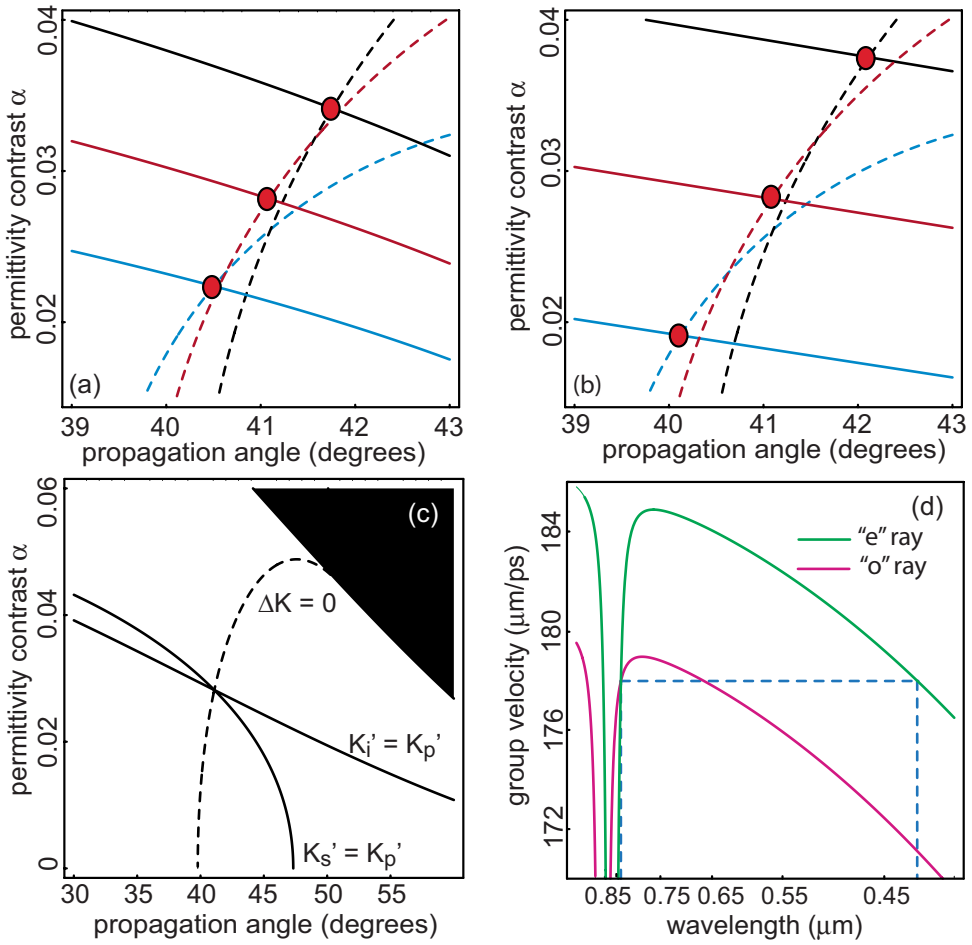

FIG. 4. (Color online) Graphical representation of (a) the conditions (i) $\Delta K=0$ and (ii) $K_p'=K_s'$, and (b) the conditions (i) $\Delta K=0$ and (ii) $K_p'=K_i'$ on $\{\alpha,\theta_{pm}\}$ space, for constant Λ [we have used the values $\Lambda=277.8$ (shown in blue), 274.9 (red), and 271.9 nm (black)]. Each intersection point indicates a solution for simultaneous phase matching and group velocity matching between the pump and one of the generated photons. (c) Graphical representation of the conditions (i) $\Delta K=0$, (ii) $K_p'=K_s'$, and (iii) $K_p'=K_i'$ on $\{\alpha,\theta_{pm}\}$ space, assuming $\Lambda=274.9$ nm. The intersection point indicates a solution for simultaneous phase matching and *complete* group velocity matching. Note that, in the shaded area, the wave number becomes complex, and therefore light does not propagate. (d) Group velocity vs frequency for the ordinary and extraordinary waves; the dotted (black) lines indicate the resulting complete group velocity matching.

group velocity matching where $K_p'=K_s'=K_i'$, or in the notation of the previous section $\tau_s^{(1)}=\tau_i^{(1)}=0$.

In order to simplify our analysis of realistic NLPCs, we first limit the parameter space; we assume that the crystal is operated at room temperature and assume a duty cycle $a/\Lambda=0.5$ throughout. Likewise, we regard the degenerate PDC frequency ω_o as a fixed parameter. It is indeed remarkable that, in general, nearly factorable PDC photon pair sources based on NLPCs permit the specification of an arbitrary central emission wavelength, and for that matter an arbitrary material, constrained only by the ability to fabricate the crystal with the required periodic index of refraction variation. Thus, for degenerate collinear PDC at a given freely specified central frequency, we are left with the following experimental parameters: Bragg period (Λ), permittivity contrast (α), crystal propagation angle (θ_{pm}), crystal length (L), and pump bandwidth (σ).

In what follows we present a numerical analysis for the simultaneous fulfillment of basic phase matching [$\Delta K^{(0)}=0$; see Eq. (18)] and complete group velocity matching [see Eq. (26)] for a one-dimensional NLPC based on a BBO crystal. Let us note that these conditions are independent of crystal length and pump bandwidth. Thus, we have three variables: Bragg period (Λ), permittivity contrast (α), and crystal propagation angle (θ_{pm}) with which to satisfy three conditions: (i) $\Delta K^{(0)}=0$, (ii) $K_p'=K_s'$, and (iii) $K_p'=K_i'$ (where the pump frequency derivatives are evaluated at $2\omega_o$ while signal and idler frequency derivatives are evaluated at ω_o).

Figure 4(a) shows in $\{\alpha,\theta_{pm}\}$ space, for three different values of Λ, the contour defined by the condition $\Delta K^{(0)}=0$ together with the contour defined by the condition $K_p'=K_s'$. Note that both contours shift as the Bragg period Λ is modified. Similarly, Fig. 4(b) shows, for the same three values of Λ, the contour defined by the condition $\Delta K^{(0)}=0$ together with the contour defined by the condition $K_p'=K_i'$. There exists a specific value of the Bragg period Λ for which the three contours meet at a single point in $\{\alpha,\theta_{pm}\}$ space, yielding the specific values of the three parameters (α, θ_{pm}, and Λ) which satisfy simultaneously phase matching and complete group velocity matching. Assuming $\lambda_o=2\pi c/\omega_0=850$ nm (which we stress may be freely specified), these values are $\alpha=0.028$, $\theta_{pm}=41.1°$, and $\Lambda=274.9$ nm, obtained numerically from the intersection of the three resulting contours [see Fig. 4(c)]. For this choice of parameters, Fig. 4(d) shows a plot of the group velocities for the ordinary and extraordinary waves. In this plot we indicate that, for a type-II interaction where the pump is an extraordinary wave and the signal and idler are extraordinary and ordinary, respectively, we indeed obtain identical group velocities for the three fields. Let us note that to our knowledge no other reported technique permits complete group velocity matching in a collinear, type-II nonlinear parametric interaction.

According to the conditions derived in the previous section, in order to guarantee factorability we require the fulfillment of the weak dispersion condition [see Eq. (29)], in ad-

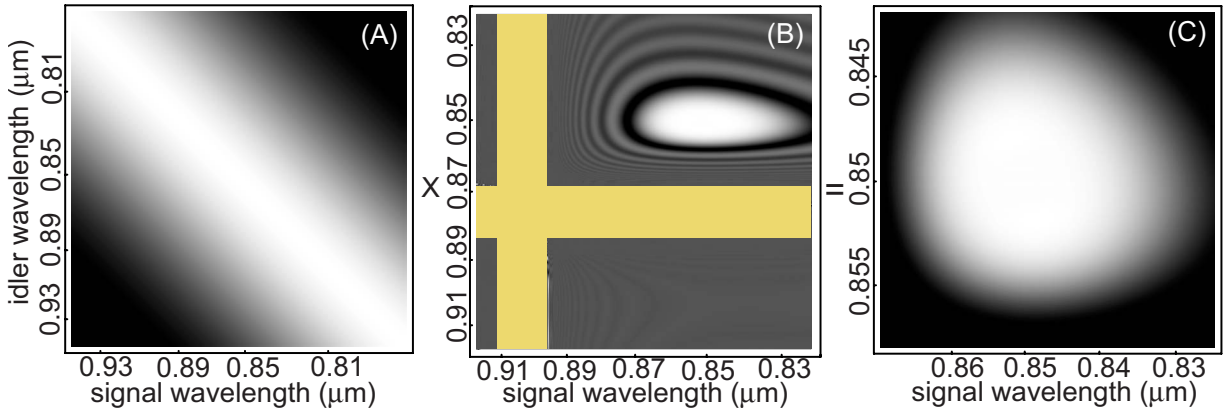

FIG. 5. (Color online) Joint spectral intensity, where dispersive effects to all orders are included and where the Gaussian approximation has not been used. (a) Pump spectral envelope with FWHM bandwidth of 10 nm. (b) Phase-matching function; the two yellow (light gray) bands indicate the band gaps for each of the two polarizations. (c) Joint spectral intensity, given as the product of the pump envelope and phase-matching function.

dition to complete group velocity matching. In particular, if this condition is satisfied for $j=2$, then three of the four remaining mixed terms in the joint spectral amplitude (to fourth order in the detunings) are suppressed. As illustrated by Fig. 2, when the signal and idler frequencies are in proximity to one of the band-gap boundaries while the pump experiences essentially only the material dispersion, group velocity dispersion and higher-order terms associated with the generated light will be greatly enhanced with respect to corresponding pump quantities. Thus, for the specific experimental parameters yielding complete group velocity matching (see the previous paragraph), the resulting second-order dispersion coefficients are $\tau_s^{(2)}=6.12$ fs^2, $\tau_i^{(2)}=0.87$ fs^2, and $\tau_p^{(2)}=0.16$ fs^2. The condition $|\tau_p^{(2)}| \ll |\tau_s^{(2)}|, |\tau_i^{(2)}|$ will be more accurately satisfied the closer the degenerate PDC frequency is to the band-gap boundaries for each polarization. However, note that, because the band-gap boundaries for the two polarizations are spectrally distinct, the weak pump dispersion condition cannot be satisfied to the same degree for both photons. Thus, for this specific choice of parameters, while the three mixed terms proportional to $\tau_p^{(2)}$ are reduced, they cannot be suppressed perfectly.

The third condition for factorability derived in the previous section, apart from complete group velocity matching and weak pump dispersion, is that the pump should be sufficiently broadband [see Eq. (24)]. Note that, while the Bragg period, permittivity contrast, and crystal propagation angle must have specific values in order to guarantee complete group velocity matching, the pump bandwidth and crystal length must satisfy a comparatively soft condition given as the inequality in Eq. (32). Figure 5 represents the resulting joint spectral intensity $|\alpha_p(\omega_s+\omega_i)\phi_{000}(\omega_s,\omega_i)|^2$, for a pump centered at $\lambda_p=2\pi c/(2\omega_o)=425$ nm with a full width at half maximum (FWHM) bandwidth of 10 nm, with crystal length $L=4$ mm, and where the rest of the parameters are as specified above, in the context of Fig. 4. Note that in this plot we have taken into account the complete dispersion (rather than a truncated power series approach) and have not used the Gaussian approximation. While these approximations were essential for our analysis, it is important to verify the degree of factorability in a two-photon state produced by a realistic source. Figure 5(a) shows the pump spectral envelope $\alpha_p(\omega_s+\omega_i)$ as given by Eq. (21), Fig. 5(b) shows the phase-matching function $\phi_{000}(\omega_s,\omega_i)$ as given by Eq. (15), and Fig. 5(c) shows the joint spectral intensity. It is apparent from the figure that the resulting two-photon state is nearly factorable. Indeed, a numerical Schmidt decomposition [23] yields a Schmidt number of $K\approx 1.11$ (which could be reduced further by moderate spectral filtering).

As has already been discussed, the effective control over group velocity properties permitted by photonic crystal structures, which may be exploited to obtain nearly factorable two-photon states, enhances higher-order dispersion terms. This has the effect that, when complete group velocity matching is not satisfied, the contours of equal amplitude of the phase-matching function in $\{\omega_s,\omega_i\}$ space tend to be highly curved. Therefore, the technique presented here is not naturally suited for the generation of states exhibiting strict correlation or anticorrelation in frequency, unless the bandwidth of interest is small enough that the curvature of the phase-matching function may be neglected.

For practical implementations of this technique, it is important to analyze the required tolerances for the experimental parameters, in order to ensure factorizability. Figure 6 shows a plot of the Schmidt number K as a function of the three parameters which must satisfy a strict condition in order to attain complete group velocity matching. We plot the Schmidt number as a function of each of these parameters, while maintaining all others equal to their nominal values (which yield the minimum value of K). Thus, Fig. 6(a) shows K vs the Bragg period Λ, Fig. 6(b) shows K vs the permittivity contrast α, and Fig. 6(c) shows K vs the crystal propagation angle θ_{pm}. We define the tolerance in variable x as $\Delta x=x_2-x_1$ where $x_{1,2}$ (with $x_2>x_1$) are the values where K rises to $K=\sqrt{2}K_{min}$ in terms of the value of the Schmidt number attained when all variables are equal to their nominal values K_{min}. Thus, we obtain $\Delta\Lambda\approx 1.04$ nm, $\Delta\alpha\approx 0.011$, and $\Delta\theta_{pm}\approx 1.23°$.

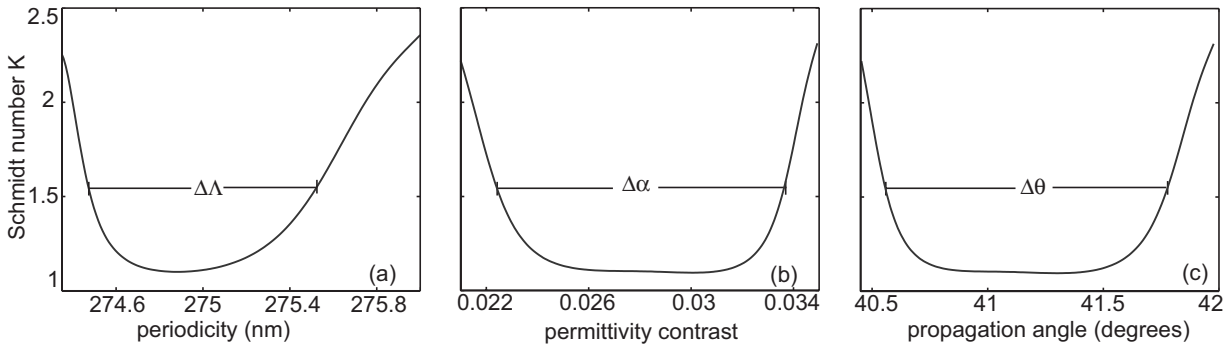

FIG. 6. Schmidt number K plotted vs (a) Bragg period Λ, (b) permittivity contrast α, and (c) crystal propagation angle θ_{pm}.

VI. CONCLUSIONS

We have studied the generation of photon pairs by spontaneous parametric down-conversion in a one-dimensional nonlinear photonic crystal, with a broadband pump. We have considered a NLPC based on a standard $\chi^{(2)}$ crystal with uniaxial birefringence where the dispersion for both polarizations has been altered from its natural state so that, throughout the length of the resulting crystal, the index of refraction for each polarization alternately takes the value consistent with material-only dispersion and a value that is larger than the former, consistent with a small permittivity contrast. We have developed a set of conditions that must be satisfied in order to guarantee a nearly factorable two-photon state. These conditions are (i) complete group velocity matching, where the pump pulse and the signal and idler photons propagate at the same group velocity [see Eq. (26)], (ii) weak pump dispersion [characterized by coefficients $\tau_p^{(j)}$; see Eq. (19)], relative to signal and idler dispersion [characterized by coefficients $\tau_{s,i}^{(j)}$; see Eq. (29)], and (iii) sufficient pump bandwidth [see Eq. (32)]. We have shown that the strongly modified dispersion in the spectral vicinity of the band-gap boundaries in a NLPC may be exploited in order to satisfy condition (i), and to partially satisfy condition (ii). The essential advantage of this technique is that for an arbitrary nonlinear material operated at an arbitrary spectral range it is in principle possible to design a photonic-crystal structure which counteracts the material dispersion so as to permit the generation of nearly factorable photon pairs in a type-II degenerate, collinear geometry which is compatible with waveguiding and which permits high-efficiency photon pair splitting. It is, however, anticipated that the fabrication of the appropriate photonic-crystal structure may pose the main technical challenge in practical implementations. Longer Bragg periods, potentially more easily fabricated, could be exploited through higher-order band gaps. It is expected that this work may be important for the development of optimized nonclassical light sources for quantum-information processing.

ACKNOWLEDGMENTS

This work was supported by Conacyt Grant No. 46370-F and UC-MEXUS Grant No. CN-06-82.

[1] See, for example, the review by P. Kok, W. J. Munro, K. Nemoto, T. C. Ralph, J. P. Dowling, and G. J. Milburn, Rev. Mod. Phys. **79**, 135 (2007).
[2] J. W. Pan, D. Bouwmeester, H. Weinfurter, and A. Zeilinger, Phys. Rev. Lett. **80**, 3891 (1998).
[3] D. Bouwmeester *et al.*, Nature (London) **390**, 575 (1997).
[4] A. B. U'Ren, C. Silberhorn, K. Banaszek, I. A. Walmsley, R. Erdmann, W. P. Grice, and M. G. Raymer, Laser Phys. **15**, 1 (2005).
[5] P. P. Rohde, W. Mauerer, and C. Silberhorn, New J. Phys. **9**, 91 (2007).
[6] A. B. U'Ren, Y. Jeronimo-Moreno, and H. Garcia-Gracia, Phys. Rev. A **75**, 023810 (2007).
[7] W. P. Grice, A. B. U'Ren, and I. A. Walmsley, Phys. Rev. A **64**, 063815 (2001).
[8] V. Giovannetti, L. Maccone, J. H. Shapiro, and F. N. C. Wong, Phys. Rev. Lett. **88**, 183602 (2002).
[9] O. Kuzucu, M. Fiorentino, M. A. Albota, F. N. C. Wong, and F. X. Kaertner, Phys. Rev. Lett. **94**, 083601 (2005).
[10] J. P. Torres, F. Macia, S. Carrasco, and L. Torner, Opt. Lett. **30**, 314 (2005).
[11] M. Hendrych, M. Micuda, and J. P. Torres, e-print arXiv:quant-ph/0612135.
[12] M. G. Raymer, J. Noh, K. Banaszek, and I. A. Walmsley, Phys. Rev. A **72**, 023825 (2005).
[13] Z. D. Walton, A. V. Sergienko, B. E. A. Saleh, and M. C. Teich, Phys. Rev. A **70**, 052317 (2004).
[14] A. B. U'Ren, K. Banaszek, and I. A. Walmsley, Quantum Inf. Comput. **3**, 480 (2003).
[15] A. B. U'Ren, R. K. Erdmann, M. de la Cruz-Gutierrez, and I. A. Walmsley, Phys. Rev. Lett. **97**, 223602 (2006).
[16] M. J. A. de Dood, W. T. M. Irvine, and D. Bouwmeester, Phys. Rev. Lett. **93**, 040504 (2004).
[17] W. T. M. Irvine, M. J. A. de Dood, and D. Bouwmeester, Phys. Rev. A **72**, 043815 (2005).
[18] M. Centini, J. Perina, Jr., L. Sciscione, C. Sibilia, M. Scalora, M. J. Bloemer, and M. Bertolotti, Phys. Rev. A **72**, 033806 (2005).

[19] J. Perina, Jr., M. Centini, C. Sibilia, M. Bertolotti, and M. Scalora, Phys. Rev. A **73**, 033823 (2006).
[20] A. N. Vamivakas, Bahaa E. A. Saleh, Alexander V. Sergienko, and Malvin C. Teich, Phys. Rev. A **70**, 043810 (2004).
[21] A. B. U'Ren, C. Silberhorn, K. Banaszek, and I. A. Walmsley, Phys. Rev. Lett. **93**, 093601 (2004).
[22] A. Yariv and P. Yeh, *Optical Waves in Crystals* (John Wiley and Sons, New York, 1984).
[23] C. K. Law, I. A. Walmsley, and J. H. Eberly, Phys. Rev. Lett. **84**, 5304 (2000).